

# Stress Analysis of Pressurized Thick Truncated conical shells with varying Modulus of Elasticity as Power Function

P Aravinda sai murthy<sup>1</sup> and Dr N.D. Mittal<sup>2</sup>

<sup>1</sup>Department of Mechanical Engineering, Maulana Azad National Institute of Technology, Bhopal (M.P.), India, 462003

<sup>2</sup>Department of Mechanical Engineering, Maulana Azad National Institute of Technology, Bhopal (M.P.), India, 462003

## Abstract

Finite element method is applied using Ansys14.0 Mechanical APDL for axisymmetric thick walled truncated cone made of Functionally Graded Material (FGM). The cone has finite length, and is subjected to axisymmetric hydrostatic internal pressure. The material is assumed to be isotropic with constant poisson's ratio and radially continuously varying elastic modulus along the thickness with a power function. The cones of varied dimensions i.e. (i) Changing the cone angle keeping the length, thickness and small base radii constant (ii) Change in length keeping the base radii and thickness constant. Using this method the truncated cone under generalized clamped-clamped conditions has been solved and the homogeneity on the stress and displacement has been investigated. FGM's with increasing as well as decreasing values of Young's modulus are considered and their results are compared. Results show that the distribution of stresses near the small and large bases of the cone are quite different compared to the remaining portion.

**Keywords:** Thick truncated cone, FGMs, Ansys, Stresses, Displacements, semi-cone angle, cone length.

## 1. Introduction

Various scientific studies are being done on shells, resulting in numerous theories about the behavior of different kinds of shells. Truncated conical shells have widely been applied in many fields such as space flight, rocket, shuttle cones, aviation, submarine technology and other civil, mechanical & aerospace engineering structures. Axisymmetric hollow truncated cones are important in contemporary industrial engineering applications such as hoppers, vessel heads, components of missiles and spacecraft. In order to optimize the weight, mechanical strength or displacement, shells with functionally graded material (FGMs) can be preferred. Functionally graded materials (FGMs) are advanced composite materials in which the material properties vary continuously from one surface to the other. The concept of FGMs was first introduced by a group of materials scientists in Japan [1-2]. FGMs are usually made of combined ceramic-metal material to

achieve the desired properties. The continuous variation of the material properties eliminates interface problems and yields more smooth stress distribution. FGMs have been used in numerous applications because of their high mechanical strength. However, investigations in FG conical shells under different mechanical loading are scarce. To date, a wide range of studies has been carried out on stress analysis of FGM cylinders [3-15].

Assuming the cone is to be long and the angle of the lateral side with a horizontal plane is large, Hausenbauer and Lee [16] without considering shear stress obtained the radial, tangential and axial wall stresses in a thick walled cone under internal and/or external pressure. Raju et al. [17] proposed a conical element for analysis of conical shells. Takahashi et al. [18] obtained the solution of free vibration of conical shells using the shear deformation theory (SDT) and frobenius series. Sundara siva rao and Ganesan [19] analyzed a conical shell under pressure using the finite element method. Using Green's function, Tavares [20] determined the stresses, strains and displacements of a thin conical shell with constant thickness and axisymmetric load. Cui et al. [21] used a new transformation for solving the governing equations of thin conical shells. The obtained equation is an ordinary differential equation with complex coefficients. Thermally induced dynamic instability of laminated composite conical shells subjected to static and periodic thermal loads using multiple scale method of perturbation theory was given by Wu and Chiu [22]. Pinto Correia et al. [23] used FEM for analysis of a composite conical shell where the shear deformation theory has been used for formulation. Wu et al. [24] gave the 3-D solution of laminated conical shells subjected to axisymmetric loadings using perturbation technique. Eipakchi et al. [25] used the mathematical approach based on the perturbation theory, for the elastic analysis of a thick truncated conical shell with varying thickness under non-uniform internal pressure. Ghannad et al. [26], based on first shear deformation theory and the

principle of virtual work obtained an elastic solution for thick truncated conical shells. Using third order shear deformation theory, an analytical solution presented for stresses and displacements in a thick conical shell with varying thickness under non uniform pressure [27]. Rayleigh-ritz energy formulation of FEM is applied to obtain the elastic behavior of the FG thick truncated cone [28]. Making use of FSDT and the virtual work principle, Ghannad and Zamani Nejad [29] derived the governing differential equations of the homogenous and isotropic axisymmetric thick-walled cylinders with same boundary conditions at the two ends. Using disk form multilayers, Nejad et al. [30] derived a semi analytical solution for determination of displacements and stresses in a rotating cylindrical shell with variable thickness under uniform pressure. Dr. N. D. Mittal, P Aravinda Sai Murthy worked on Stress Analysis of Pressurized Thick Truncated Conical Shells with varying Modulus of Elasticity as Power Function. [32]

In the present study, stress and displacement distribution along the geometry of the axisymmetric thick walled cone with finite length under internal hydrostatic pressure for varied dimensions by changing semi-cone angle and length of the cone are dealt. The solution is obtained from the Finite Element Analysis using Ansys14.0 Mechanical APDL.

## 2. Geometry and material gradient

### 2.1. Geometry of truncated thick hollow cone

The geometry of the thick truncated hollow cone is as shown in the fig.1, where  $h$  is the thickness of the cone,  $a$  and  $b$  are the radius of large and small base of the cone respectively,  $L$  is the length and  $\Phi$  is the semi-vertex angle of the cone.  $R_i$  and  $z$  are the axis of cylindrical coordinate system.

The location of a typical point  $m$ , with in the shell element may be determined by  $R_i$  and  $z$ , as

$$m: (r, x) = (R_i(x) + z, x) \quad (1)$$

Where  $R_i$  represents the distance of internal surface from the central axis and  $z$  is the distance of typical point from the internal surface.

$$R_i(x) = a - (a - b) \frac{x}{L} \quad (3.1.1)$$

$$R_i(x) = a - (\tan \Phi) x \quad (3.1.2)$$

In Eq. (1),  $x$  and  $z$  must be within the following ranges

$$\left. \begin{aligned} 0 \leq x \leq L \\ 0 \leq z \leq h \end{aligned} \right\} \quad (2)$$

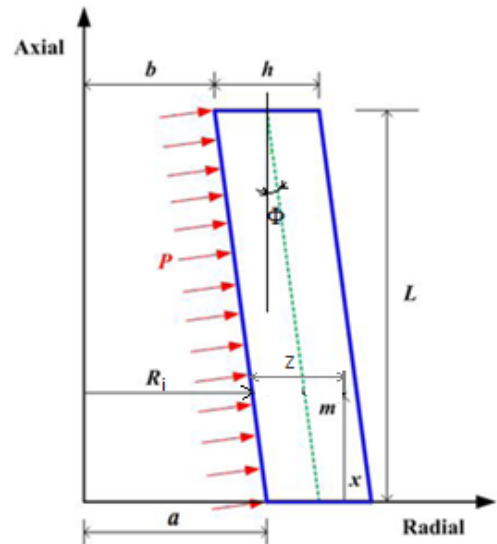


Fig. 1 Geometry of the cone

### 2.2. Material gradient

The cones material is grade though the  $x$  direction. The cone is made of a combine ceramic-metal material and the material composition varies continuously along its thickness i.e. radial direction. The inner surface of the cone is pure ceramic, and the outer surface is pure metal. The material distribution can be mathematically expressed [31] as follows

$$E = E_c + (E_m - E_c) \left(\frac{z}{h}\right)^n \quad (4)$$

Where “ $z$ ” is the normal distance of the points through the thickness of the cone from the inner surface.  $E$  is the Young’s modulus;  $n$  is a non-negative exponent. Subscripts “ $c$ ” and “ $m$ ” stand for ceramic and metal respectively.

On the internal surface  $z$  is taken as zero and reaches the value equal to  $h$  at the external surface. Therefore, several isotropic layers with varying material properties via power law are laid one over the other to get a composite structure. For  $n > 0$  young’s modulus decreases from inner to outer surface for the given values of  $E_m$  and  $E_c$ .

If the material properties are taken in such a way that the inner surface is a metal and the outer

surface to be a ceramic, then the inverse distribution can be seen. Here the exponent  $m$  in Eq. (5) is similar to that of  $n$  in Eq. (4). For  $m > 0$  young's modulus increases from inner to outer surface.

$$E = E_m + (E_c - E_m) \left(\frac{z}{h}\right)^m \quad (5)$$

The distribution of young's modulus along the thickness for the assumed values (0, 1, and 2, 3) of  $n$  and  $m$  is depicted in fig.2.

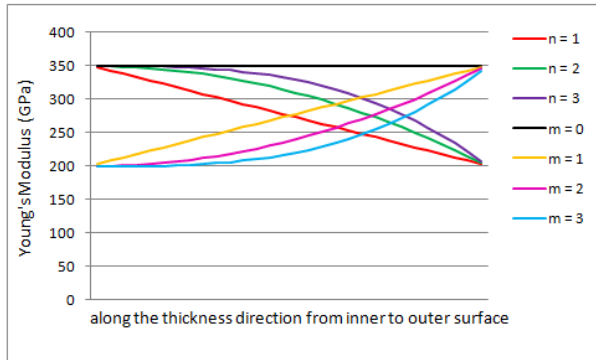


fig.2 distribution of Young's modulus

fig.2 gives the distribution of young's modulus ranging from 200GPa to 350GPa of a cone with thickness  $h = 20\text{mm}$  along the radial direction. For  $n$  or  $m$  equals to zero the material is homogenous with  $E$  equal to 200GPa & 350GPa respectively.

### 3. Analysis in Ansys Mechanical APDL

Ansys 14.0 Mechanical APDL package was used in the Static Analysis of thick hollow truncated cone with constant thickness to get the values of stresses and displacements. Solid 8 node 183 element in axisymmetric mode, which is an element with eight nodes and two degrees of translational degrees of freedom in the axial and radial direction per each node, was used for modeling.

In order to consider the variation of material property (Young's modulus) along the thickness of the conical shell with a power function, thickness of the cylinder is divided to some homogenous layers. Each layer's material property have been defined as the power function of the distance from inner layer. Finally the conical shell consists of some coherent homogenous layers whose properties at the contact location of the layers (along the length) are the average of left and right limit of two layer boundaries.

Several homogeneous models with varying number of elements along the axial direction by

fixing the number of elements (30 layers) along the radial direction were analyzed.

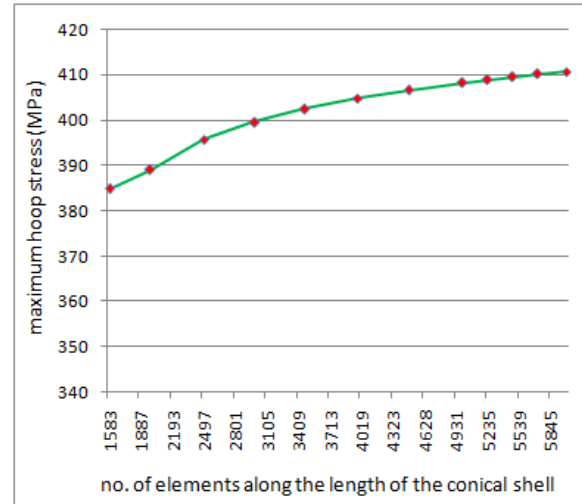


fig.3 distribution of Maximum hoop stress with respect to no. of elements along the axial direction

Finally optimal number of elements are chosen by the convergence test performed via graphical plot made as showed in fig.3. Internal hydrostatic pressure is applied to the nodes of inner layer. Nodes around the two ends of the conical shell are constrained from movement by clamped boundary condition. In the next sections the numerical results have been investigated for thick conical shell under internal pressure with clamped-clamped boundary condition.

### 4. Results and Discussion

As a case-study, we consider a thick truncated cone whose elastic modulus varies along the radial direction and has the following characteristics:

internal radius at the larger base ( $a$ ) = 40mm

internal radius at the smaller base( $b$ )= 30mm

thickness ( $h$ ) = 20mm

axial length ( $L$ ) = 400mm

internal pressure ( $P$ ) = 80MPa

no. of elements in the axial direction = 6000

no. of elements in the radial direction = 30

Young's Modulus:

$E_m = 200 \text{ GPa}$ ,  $E_c = 350 \text{ GPa}$

Poisson's ratio ( $\mu$ ) = 0.3

#### 4.1. Stress Analysis of hollow Truncated FGM cones by varying semi-cone angle ( $\Phi$ ) with fixed length (L), thickness (h) and base radius (b)

Stress analysis has been done by varying the dimensions of the hollow cone. The cones (a), (b) & (c) of fig.4 have same height (= 400 mm), same thickness (= 20 mm) and same radii (at the smaller base, which are 30mm internal and 50mm external). Young's modules for all the cones are same as mentioned in the section 2.2. The internal base circle radius of the larger base of the cones (a), (b) & (c) are 40mm, 70mm and 90mm respectively. And the semi-cone angles are changed to  $1.43210^\circ$ ,  $5.71059^\circ$  and  $9.92624^\circ$  respectively.

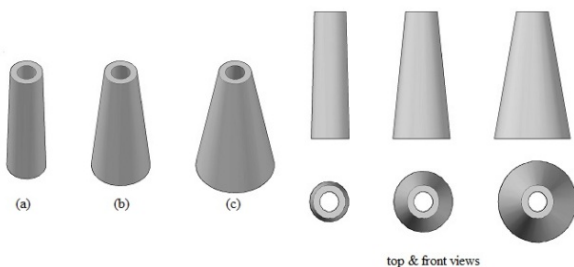


fig.4 FGM cones of varied cone angle( $\Phi$ ) with fixed length(L), thickness (h) and small base radius(b)

##### 4.1.1. Displacement distribution

###### 4.1.1.1. Radial displacement

The set of graphs (fig.5 to fig.7) are the plot between the radial displacement and the length of the cone along the middle layer in the axial direction (from bottom (larger base) to top (small base)) with respect to change in the semi-cone angle. Radial displacement (along the middle layer in axial direction) increases rapidly (from the larger base) attains a maximum value near to the larger base and then slowly reduces (till the near end of the smaller base). From the graphs we can infer that, as the angle of the cone increases radial displacements increases. Negligible change in displacements is observed at the top portion of the cone. whereas, change in displacements is high at the bottom portion (with respect to change the semi-cone angle). Displacement for m series is greater than that of n series. Whereas the displacement for homogenous material ( $m=0$ ) is the least. Variation trend of the radial displacement is same with respect to change in the semi-cone angle.

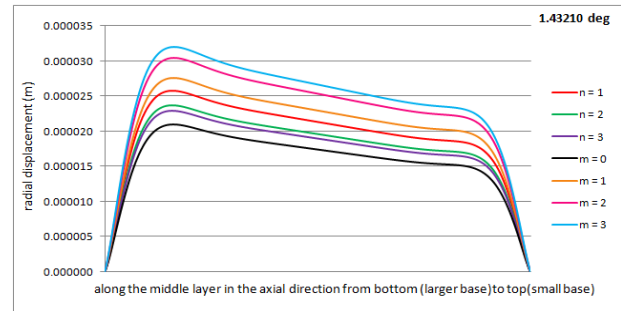


fig.5 distribution of radial displacement along the middle layer in the axial direction from bottom (larger base) to top (small base) for  $\Phi= 1.43210^\circ$

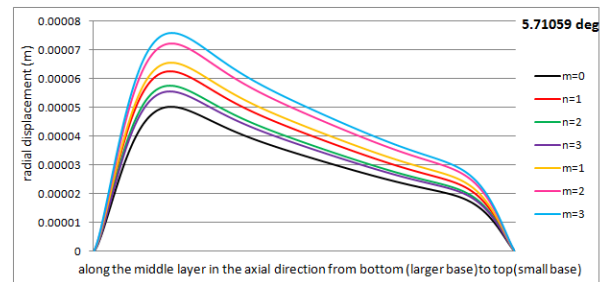


fig.6 distribution of radial displacement along the middle layer in the axial direction from bottom (larger base) to top (small base) for  $\Phi= 5.71059^\circ$

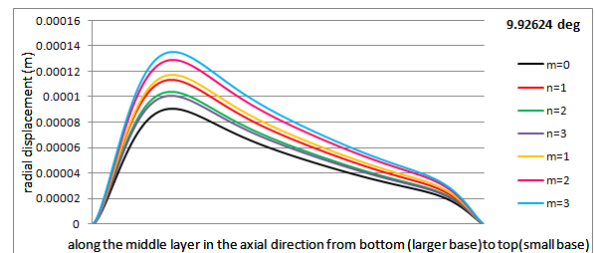


fig.7 distribution of radial displacement along the middle layer in the axial direction from bottom (larger base) to top (small base) for  $\Phi= 9.92624^\circ$

The set of graphs (fig.8 to fig.10) are the plot between the radial displacement and the thickness of the cone along the middle layer in the radial direction from internal to external surface with respect to change in the semi-cone angle. Radial displacement gradually reduces from internal to external surface (at the middle of the cone) along the thickness of the cone. From the graphs we can infer that, as the angle of the cone increases, radial displacements increases. Displacement for m series is greater than that of n series. Whereas the displacement for homogenous material ( $m=0$ ) is the least. Variation trend of the radial displacement is same with respect to change in the semi-cone angle.

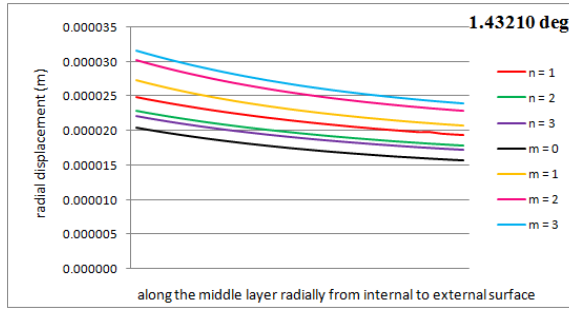


fig.8 distribution of radial displacement along the middle layer from internal to the external surface  $\Phi= 1.43210^0$

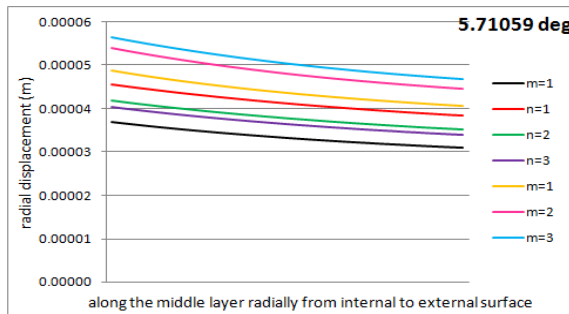


fig.9 distribution of radial displacement along the middle layer from internal to the external surface  $\Phi= 5.71059^0$

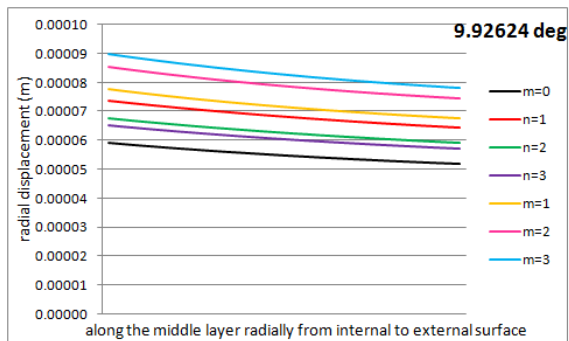


fig.10 distribution of radial displacement along the middle layer from internal to the external surface  $\Phi= 9.92624^0$

#### 4.1.1.2. Axial displacement

The set of graphs (fig.11 to fig.13) are the plot between the Axial displacement and the length of the cone along the middle layer in the axial direction (from bottom (larger base) to top (small base)) with respect to change in the semi-cone angle. Axial displacement increases and reaches to a maximum value (to the near end of the larger base) and reduces slowly and reach to zero value (to the near end of the smaller base). For lower cone angles, we can observe the occurrence of negative displacements at the extreme top portion. Axial displacement increases with the increase the semi-cone angle. Displacement

for m series is greater than that of n series. Whereas the displacement for homogenous material (m=0) is the least. Variation trend of the axial displacement is same with respect to change in the semi-cone angle.

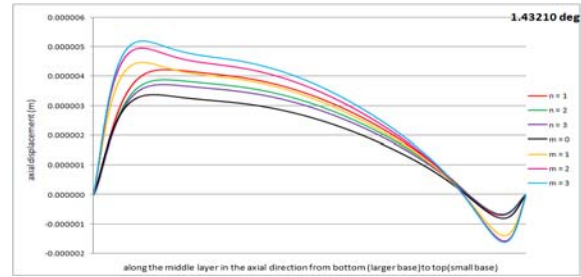


fig.11 distribution of axial displacement along the middle layer in the axial direction from bottom(larger base) to top(small base) for  $\Phi= 1.43210^0$

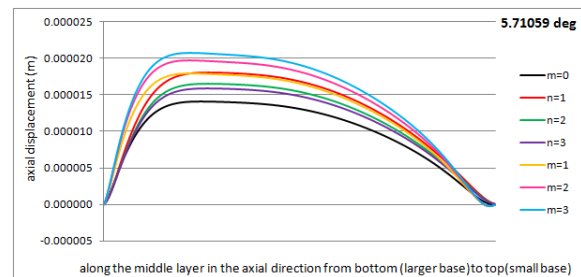


fig.12 distribution of axial displacement along the middle layer in the axial direction from bottom(larger base) to top(small base) for  $\Phi= 5.71059^0$

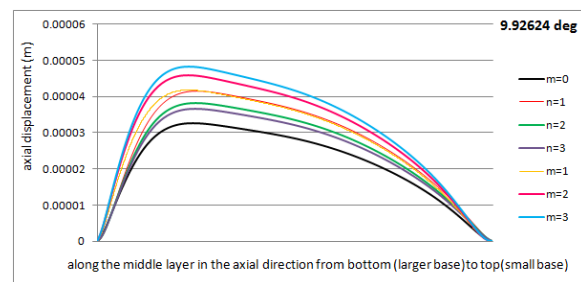


fig.13 distribution of axial displacement along the middle layer in the axial direction from bottom(larger base) to top(small base) for  $\Phi= 9.92624^0$

The set of graphs (fig.14 to fig.16) are the plot between the axial displacement and the thickness of the cone along the middle layer in the radial direction from internal to external surface with respect to change in the semi-cone angle. Axial displacement gradually increases from internal to external surface (at the middle of the cone) along the thickness. From the graphs we can infer that, as the angle of the cone increases axial displacements increases. The increase is significant at the outer surface. Displacement for m series is greater than that of n series with the

exception that, displacement for  $m=1$  is less than  $n=1$ . Whereas the displacement for homogenous material ( $m=0$ ) is the least. Variation trend of the axial displacement is same with respect to change in the semi-cone angle.

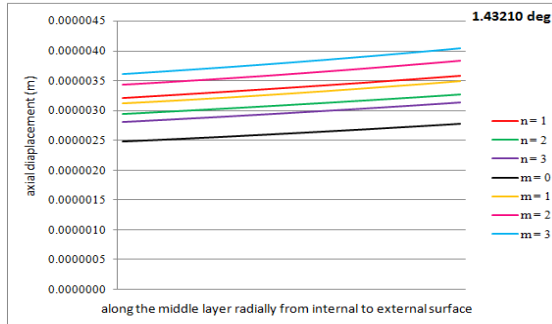


fig.14 distribution of axial displacement along the middle layer from internal to the external surface  $\Phi=1.43210^\circ$

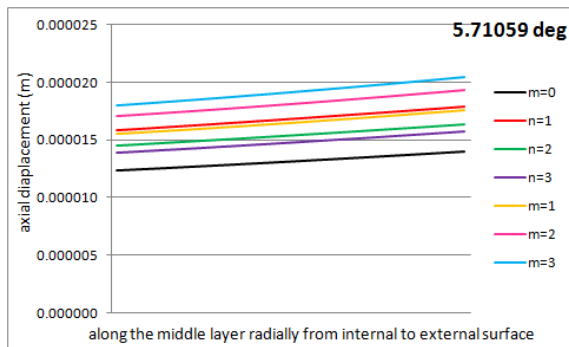


fig.15 distribution of axial displacement along the middle layer from internal to the external surface  $\Phi=5.71059^\circ$

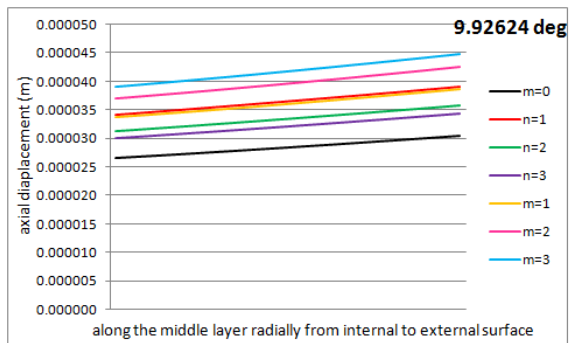


fig.16 distribution of axial displacement along the middle layer from internal to the external surface  $\Phi=9.92624^\circ$

### 4.1.2 . Stress Distribution

#### 4.1.2.1. Radial stress distribution

The set of graphs (fig.17 to fig. 19) are the plot between the Radial stress and the length of the cone along the middle layer in the axial direction (from

bottom (larger base) to top (small base)) with respect to change in the semi-cone angle. The stress induced is of compressive in nature. Maximum radial stresses are induced at the near end's of the bases. The radial stress is almost moving constant along the central portion in the middle layer along the length of the shell. As the cone angle is increased the magnitude of the compressive stress increases significantly at the extreme bottom portion. Radial stress for  $m$  series is greater than that of  $n$  series. The stress distribution of the homogeneous material is in between the distribution curves of  $(n, m) > 0$ . Variation trend of the radial stress is same with respect to change in the semi-cone angle.

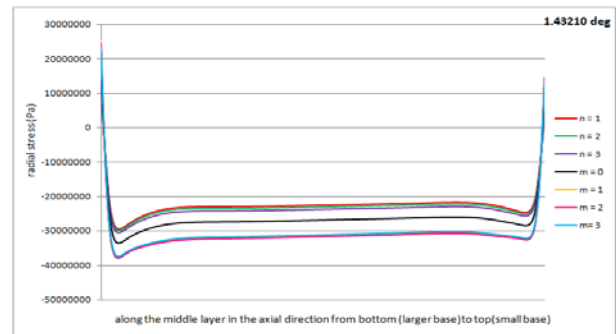


fig.17 distribution of radial stress along the middle layer in the axial direction from bottom (larger base) to top (small base) for  $\Phi=1.43210^\circ$

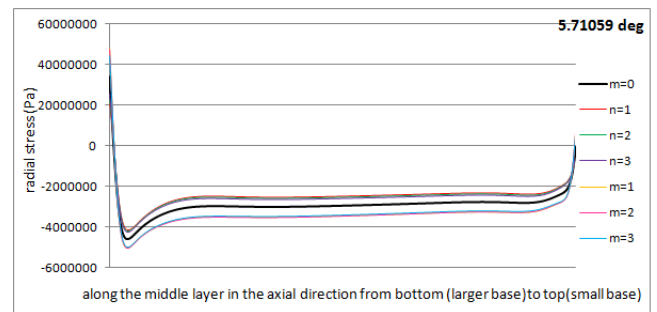


fig.18 distribution of radial stress along the middle layer in the axial direction from bottom (larger base) to top (small base) for  $\Phi=5.71059^\circ$

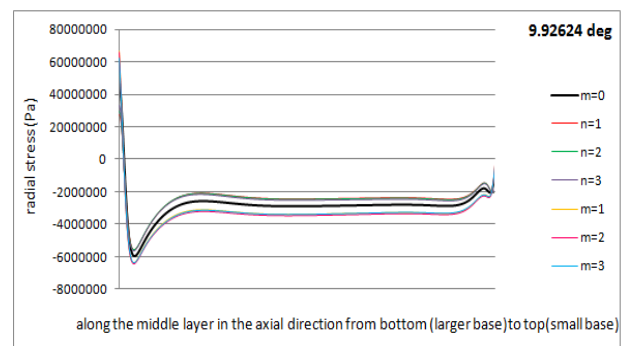


fig.19 distribution of radial stress along the middle layer in the axial direction from bottom(larger base) to top(small base) for  $\Phi=9.92624^0$

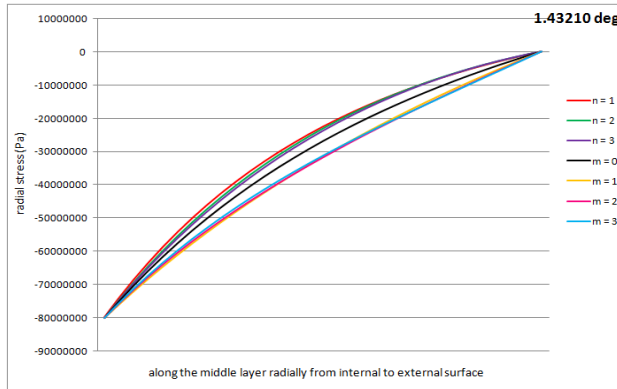


fig.20 distribution of radial stress along the middle layer from internal to the external surface  $\Phi= 1.43210^0$

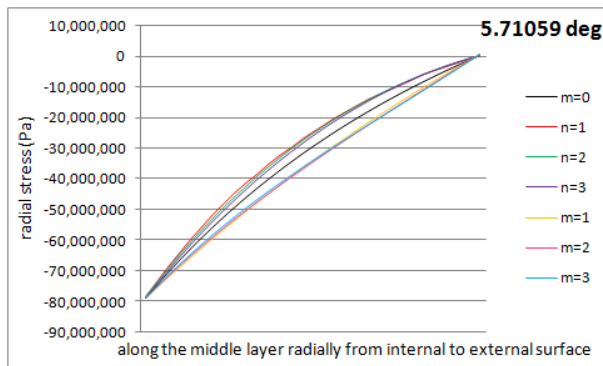


fig.21 distribution of radial stress along the middle layer from internal to the external surface  $\Phi= 5.71059^0$

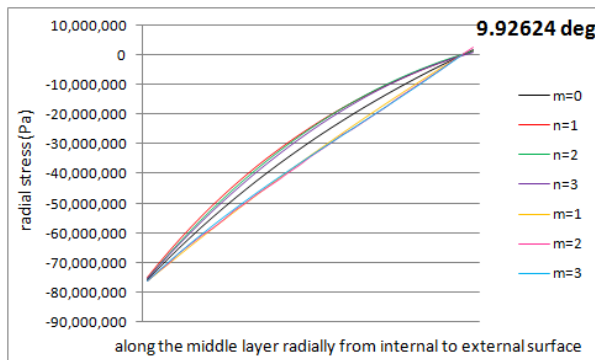


fig.22 distribution of radial stress along the middle layer from internal to the external surface  $\Phi= 9.92624^0$

The set of graphs (fig.20 to fig.22) are the plot between the radial stress and the thickness of the cone along the middle layer in the radial direction from internal to external surface with respect to change in the semi-cone angle. Radial compressive stress decreases from inner to outer end. As the cone

angle is increased the magnitude of the compressive stress is almost constant. Radial stress for m series is greater than that of n series. The stress distribution of the homogeneous material is in between the distribution curves of  $(n, m) > 0$ . Variation trend of the radial stress is same with respect to change in the semi-cone angle.

#### 4.1.2.2. Axial stress distribution

The set of graphs (fig.23 to fig. 25) are the plot between the axial stress and the length of the cone along the middle layer in the axial direction (from bottom (larger base) to top (small base)) with respect to change in the semi-cone angle. Axial stress decreases radially from inner surface to the outer surface with a fluctuation near the bases. The fluctuation of the stress is minimized at the smaller base with the increase in the semi-cone angle. Also we can observe that, as semi-cone angle increases compressive stress is induced at the smaller base. Intensity of stress increases with increase in the semi-cone angle. Stress for n series is greater than that of m series where as the trend is reversed at the ends (bases). The stress distribution of the homogeneous material is in between the distribution curves of  $(n, m) > 0$ . Variation trend of the axial stress is same with respect to change in the semi-cone angle.

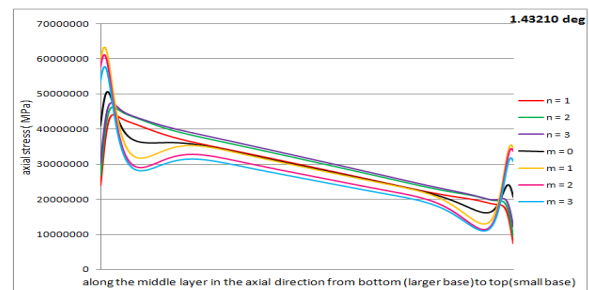


fig.23 distribution of axial stress along the middle layer in the axial direction from bottom(larger base) to top(small base) for  $\Phi= 1.43210^0$

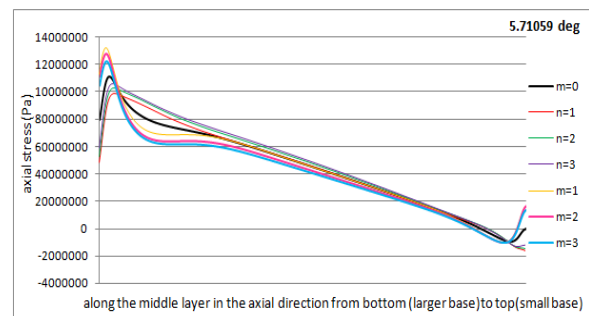


fig.24 distribution of axial stress along the middle layer in the axial direction from bottom(larger base) to top(small base) for  $\Phi=5.71059^{\circ}$

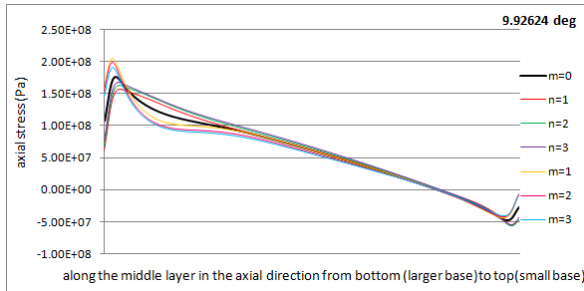


fig.25 distribution of axial stress along the middle layer in the axial direction from bottom(larger base) to top(small base) for  $\Phi=9.92624^{\circ}$

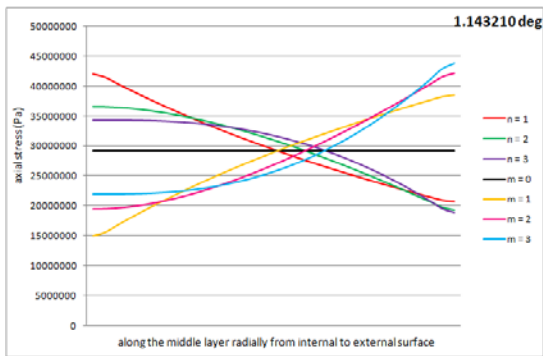


fig.26 distribution of axial stress along the middle layer from internal to the external surface  $\Phi=1.43210^{\circ}$

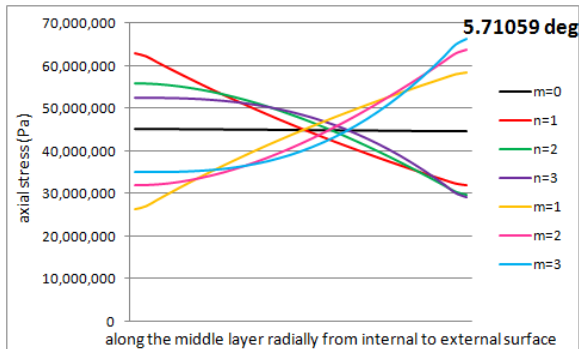


fig.27 distribution of axial stress along the middle layer from internal to the external surface  $\Phi=5.71059^{\circ}$

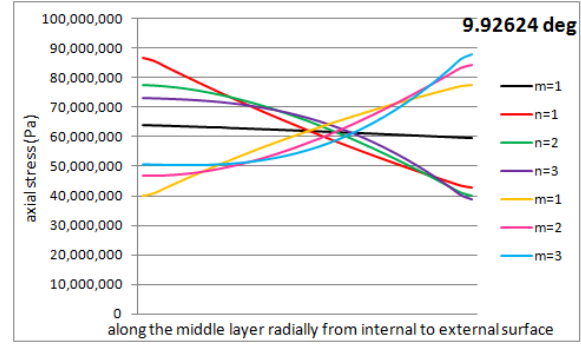


fig.28 distribution of axial stress along the middle layer from internal to the external surface  $\Phi=9.92624^{\circ}$

The set of graphs (fig.26 to fig.28) are the plot between the axial stress and the thickness of the cone along the middle layer in the radial direction from internal to external surface with respect to change in the semi-cone angle. Axial stress is more for  $n=1, 2$  &  $3$  at the inner half along the thickness ( $0$  to  $h/2$ ) and low for  $m=1, 2$  &  $3$ . The trend is reverse along outer half along the thickness ( $h/2$  to  $h$ ) i.e. the axial stress is low for  $n=1, 2$  &  $3$  and more for  $m=1, 2$  &  $3$ . The stress distribution of the homogeneous material is almost constant and it is in between the distribution curves of  $(n, m) > 0$ . Intensity of stress increases with increase in the semi-cone angle. Variation trend of the axial stress is same with respect to change in the semi-cone angle.

#### 4.1.2.3. Hoop stress distribution

The set of graphs (fig.29 to fig.31) are the plot between the hoop stress and the length of the cone along the middle layer in the axial direction (from bottom (larger base) to top (small base)) with respect to change in the semi-cone angle. Hoop stress (along the middle layer in axial direction) increases rapidly (from the larger base) attains a maximum value near to the larger base and then slowly reduces (till the near end of the smaller base) and decreases. From the graphs we can infer that, as the angle of the cone increases, hoop stress increases. Negligible change in stress is observed at the top portion of the cone (with respect to change the semi-cone angle). whereas, change in stress is high at the bottom portion. Stress for  $n$  series is greater than that of  $m$  series. The stress distribution of the homogeneous material is in between the distribution curves of  $(n, m) > 0$ . Variation trend of the hoop stress is same with respect to change in the semi-cone angle.

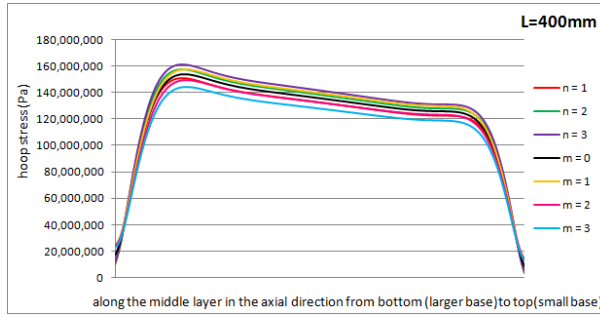


fig.29 distribution of hoop stress along the middle layer in the axial direction from bottom(larger base) to top(small base) for  $\Phi=1.43210^\circ$

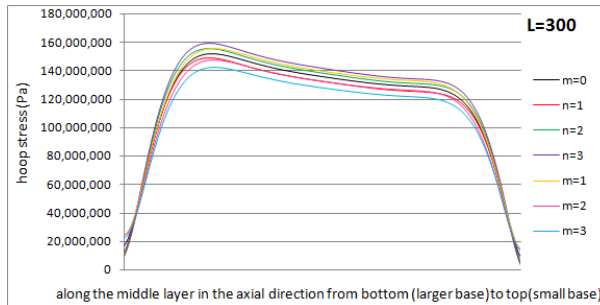


fig.30 distribution of hoop stress along the middle layer in the axial direction from bottom(larger base) to top(small base) for  $\Phi=5.71059^\circ$

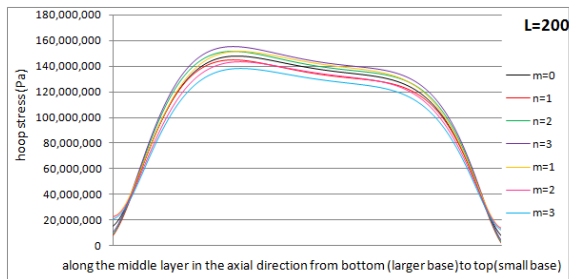


fig.31 distribution of hoop stress along the middle layer in the axial direction from bottom(larger base) to top(small base) for  $\Phi=9.92624^\circ$

The set of graphs (fig.31 to fig.33) are the plot between the hoop stress and the thickness of the cone along the middle layer in the radial direction from internal to external surface with respect to change in the semi-cone angle. Hoop stress is more for  $n=1, 2$  &  $3$  at the inner half along the thickness ( $0$  to  $h/2$ ) and low for  $m=1, 2$  &  $3$ . The trend is reverse along outer half along the thickness ( $h/2$  to  $h$ ) i.e. the axial stress is low for  $n=1, 2$  &  $3$  and more for  $m=1, 2$  &  $3$ . The stress distribution of the homogeneous material is in between the distribution curves of  $(n, m) > 0$ . Intensity of stress increases with increase in the semi-cone angle. Variation trend of the hoop

stress is same with respect to change in the semi-cone angle.

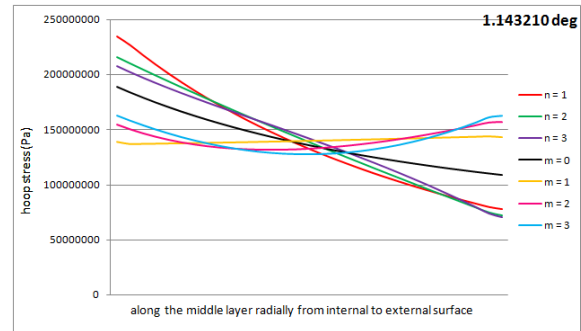


fig.31 distribution of hoop stress along the middle layer from internal to the external surface  $\Phi=1.43210^\circ$

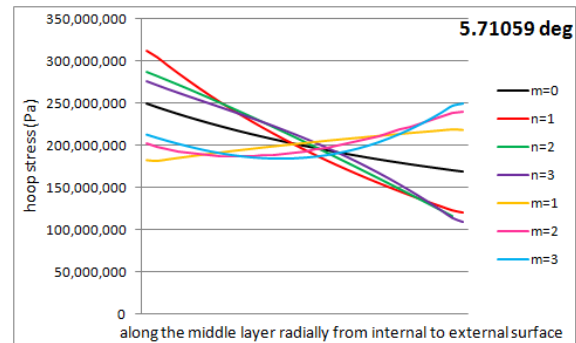


fig.32 distribution of hoop stress along the middle layer from internal to the external surface  $\Phi=5.71059^\circ$

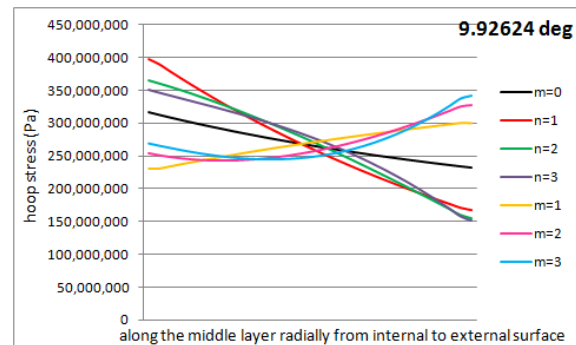


fig.33 distribution of hoop stress along the middle layer from internal to the external surface  $\Phi=9.92624^\circ$

#### 4.1.2.4. shear stress distribution

The set of graphs (fig.34 to fig.36) are the plot between the shear stress and the length of the cone along the middle layer in the axial direction (from bottom (larger base) to top (small base)) with respect to change in the semi-cone angle. Maximum stress is induced at the near end of larger base and rapidly reduces to negative shear stress. Then remains almost constant and rapidly decreases to maximum negative

stress at the smaller base. The central portion of the curve goes to intensive negative shear stress zone with the increase in the semi-cone angle. Shear stress is same for homogeneous as well as FGM's with  $(n, m) = 1, 2 \& 3$ . From the graphs we can infer that, as the angle of the cone increases, shear stress increases. Whereas change in shear stress at the smaller base is negligible. Variation trend of the shear stress is same with respect to change in the semi-cone angle.

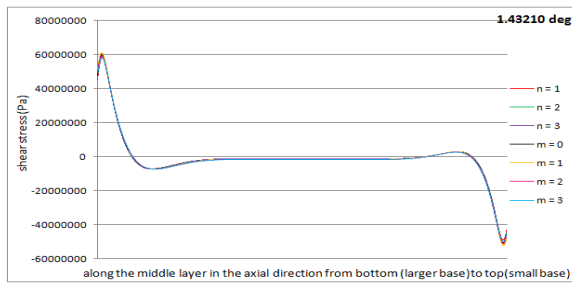


fig.34 distribution of shear stress along the middle layer in the axial direction from bottom(larger base) to top(small base) for  $\Phi=1.43210^\circ$

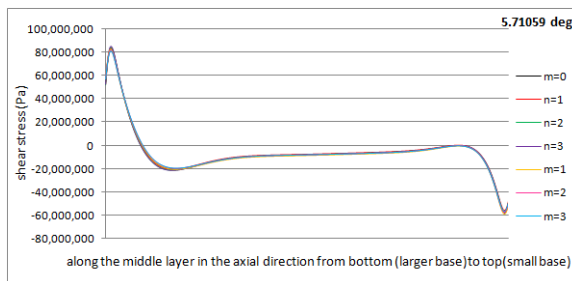


fig.35 distribution of shear stress along the middle layer in the axial direction from bottom(larger base) to top(small base) for  $\Phi=5.71059^\circ$

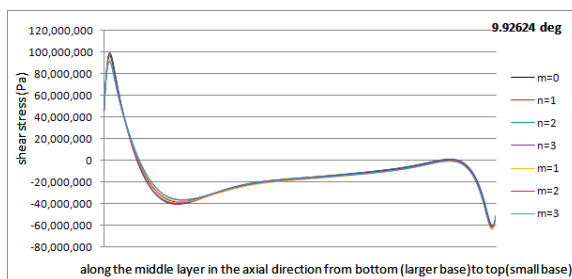


fig.36 distribution of shear stress along the middle layer in the axial direction from bottom(larger base) to top(small base) for  $\Phi=9.92624^\circ$

The set of graphs (fig.37 to fig.39) are the plot between the shear stress and the thickness of the cone along the middle layer in the radial direction from internal to external surface with respect to change in the semi-cone angle. shear stress is more for  $n=1, 2 \& 3$  at the inner half along the thickness  $(0 \text{ to } h/2)$

and low for  $m=1, 2 \& 3$ . The trend is reverse along outer half along the thickness  $(h/2 \text{ to } h)$  i.e. the axial stress is low for  $n=1, 2 \& 3$  and more for  $m=1, 2 \& 3$ . The shear stress distribution of the homogeneous material is in between the distribution curves of  $(n, m) > 0$ . Intensity of stress increases with increase in the semi-cone angle significantly near the interior surface. Variation trend of the hoop stress is same with respect to change in the semi-cone angle.

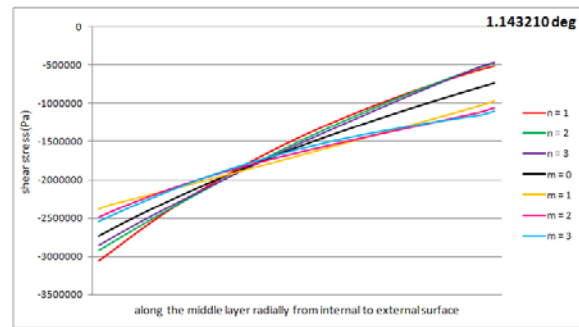


fig.37 distribution of shear stress along the middle layer from internal to the external surface  $\Phi=1.43210^\circ$

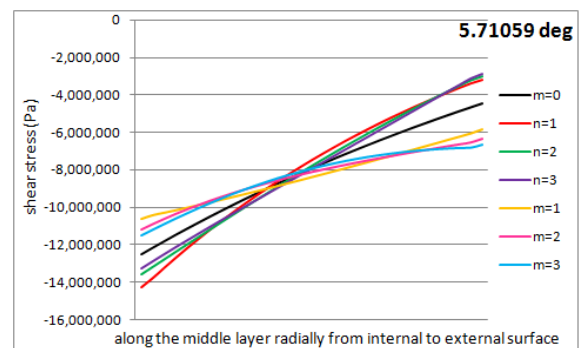


fig.38 distribution of shear stress along the middle layer from internal to the external surface  $\Phi=5.71059^\circ$

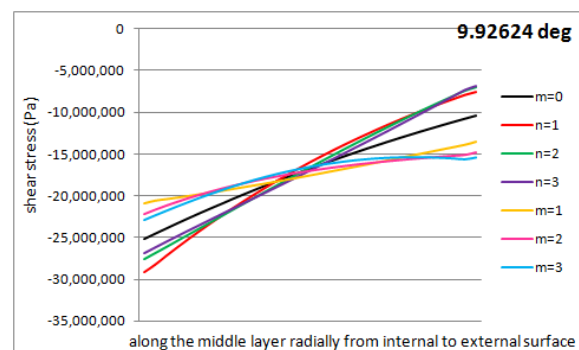


fig.39 distribution of shear stress along the middle layer from internal to the external surface  $\Phi=9.92624^\circ$

#### 4.2. Stress Analysis of hollow Truncated FGM cones of varied length with fixed base radii and thickness

The cones (a), (b) & (c) have same base radii (at the top surface, which are 30mm internal and 50mm external and at the bottom surface 40mm internal and 60mm external , same thickness (=20mm). Young's modules for all the cones are same as mentioned in the section 2.2. Lengths of the cones are varied as 400mm, 300mm and 200mm as shown in the figure 40 (a), (b) and (c).

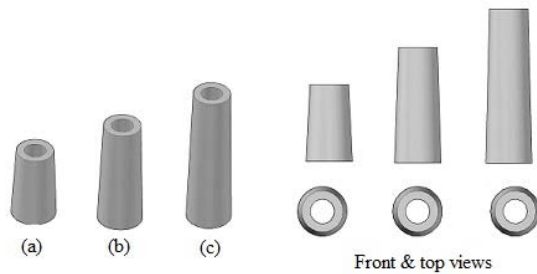


fig.40 FGM cones of varied length with fixed base radii and thickness

### 4.2.1. Displacement distribution

#### 4.2.1.1. Radial Displacement

The set of graphs (fig.41 to fig.43) are the plot between the radial displacement and the length of the cone along the middle layer in the axial direction (from bottom (larger base) to top (small base)) with respect to change in the length of the cone. Radial displacement (along the middle layer in axial direction) increases rapidly (from the larger base) attains a maximum value near to the larger base and then slowly reduces (till the near end of the smaller base) and decreases. From the graphs we can infer that, as the length of the cone increases, radial displacements decreases slightly. Change in displacements is high at the bottom and top portions (with respect to change the length of the cone). Displacement for m series is greater than that of n series. Whereas the displacement for homogenous material (m=0) is the least. Variation trend of the radial displacement is same with respect to change in the length of the cone.

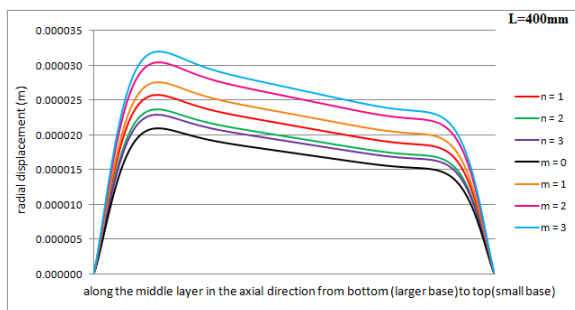


fig.41 distribution of radial displacement along the middle layer in the axial direction from bottom(larger base) to top(small base) for L=400mm

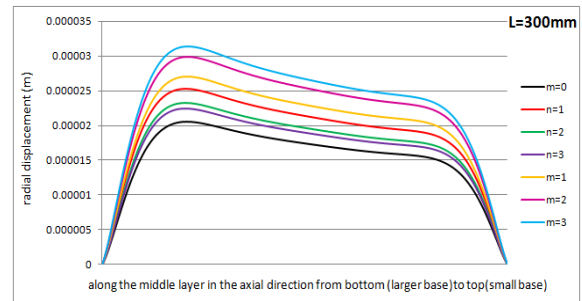


fig.42 distribution of radial displacement along the middle layer in the axial direction from bottom(larger base) to top(small base) for L=300mm

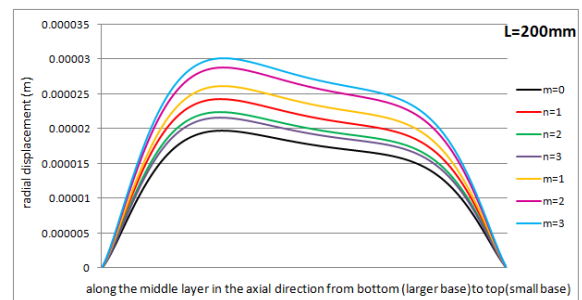


fig.43 distribution of radial displacement along the middle layer in the axial direction from bottom(larger base) to top(small base) for L=200mm

The set of graphs (fig.44 to fig.46) are the plot between the radial displacement and the thickness of the cone along the middle layer in the radial direction from internal to external surface with respect to change in the length of the cone. Radial displacement gradually reduces from internal to external surface (at the middle of the cone) along the thickness. From the graphs we can infer that, as the angle of the cone increases radial displacements slightly increases. Displacement for m series is greater than that of n series. Whereas the displacement for homogenous material (m=0) is the least. Variation trend of the radial displacement is same with respect to change in the length of the cone.

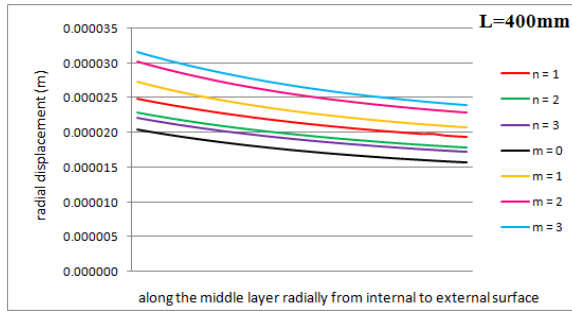


fig.44 distribution of radial displacement along the middle layer from internal to the external surface L=400mm

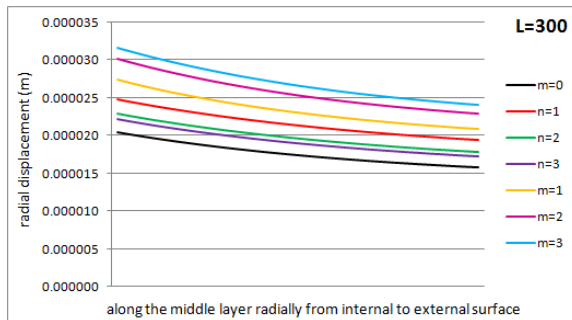


fig.45 distribution of radial displacement along the middle layer from internal to the external surface L=300mm

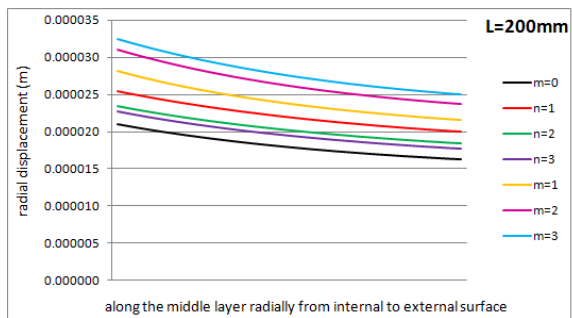


fig.46 distribution of radial displacement along the middle layer from internal to the external surface L=200mm

#### 4.2.1.2. Axial displacement

The set of graphs (fig.47 to fig.49) are the plot between the Axial displacement and the length of the cone along the middle layer in the axial direction (from bottom (larger base) to top (small base)) with respect to change in the length of the cone. Axial displacement increases and reaches to a maximum value (to the near end of the larger base) and reduces slowly and reach to zero value (to the near end of the smaller base). Axial displacement reduces with the increase the length of the cone. Displacement for m series is greater than that of n series. Whereas the displacement for homogenous material (m=0) is the least.

least. Variation trend of the axial displacement is same with respect to change in the length of the cone.

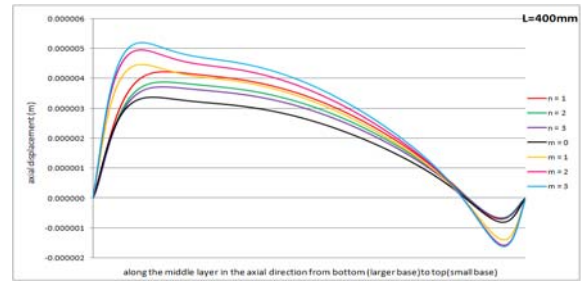


fig.47 distribution of axial displacement along the middle layer in the axial direction from bottom (larger base) to top (small base) for L=400mm

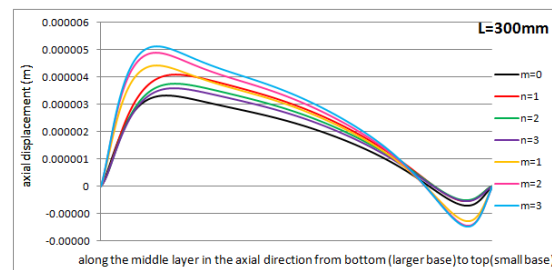


fig.48 distribution of axial displacement along the middle layer in the axial direction from bottom (larger base) to top (small base) for L=300mm

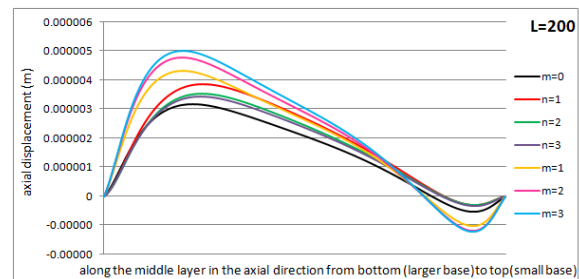


fig.49 distribution of axial displacement along the middle layer in the axial direction from bottom (larger base) to top (small base) for L=200mm

The set of graphs (fig.50 to fig.52) are the plot between the axial displacement and the thickness of the cone along the middle layer in the radial direction from internal to external surface with respect to change in the length of the cone. Axial displacement gradually increases from internal to external surface (at the middle of the cone) along the thickness. Displacement for m series is greater than that of n series with the exception that, displacement for m=1 is less than n=1. Whereas the displacement for homogenous material (m=0) is the least. From the graphs we can infer that, as the length of the cone increases axial displacements decreases. With the

increase in the length of the cone axial displacement decreases significantly at the inner surface. Variation trend of the axial displacement is same with respect to change in the length of the cone.

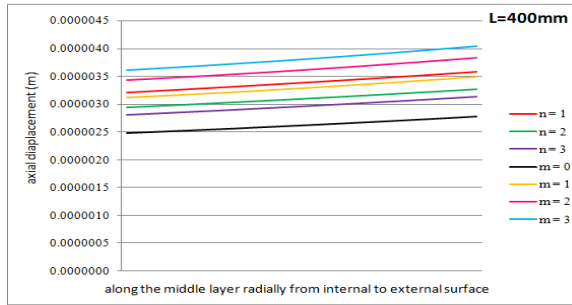


fig.50 distribution of axial displacement along the middle layer from internal to the external surface L=400mm

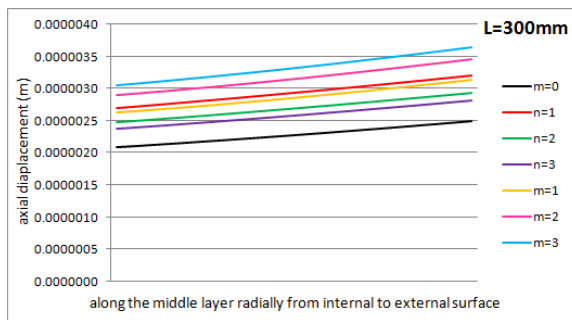


fig.51 distribution of axial displacement along the middle layer from internal to the external surface L=300mm

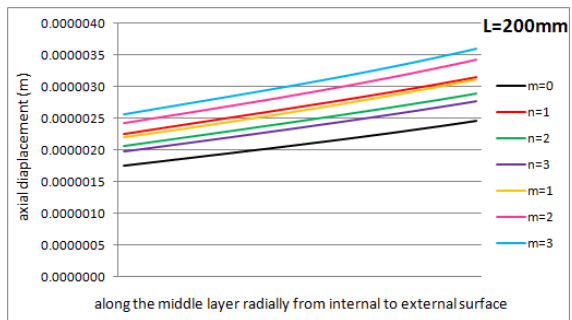


fig.52 distribution of axial displacement along the middle layer from internal to the external surface L=200mm

## 4.2.2. Stress Distribution

### 4.2.2.1. Radial stress distribution

The set of graphs (fig.53 to fig. 55) are the plot between the Radial stress and the length of the cone along the middle layer in the axial direction (from bottom (larger base) to top (small base)) with respect to change in the length of the cone. The stress induced is of compressive in nature. Maximum

radial stresses are induced at the near end's of the bases. The radial stress is almost moving constant along the central portion in the middle layer along the length of the shell. As the length of the cone is increased the magnitude of the stress increases slightly near the bases whereas remains almost constant in the remaining portion. Radial stress for m series is greater than that of n series. The stress distribution of the homogeneous material is in between the distribution curves of  $(n, m) > 0$ . Variation trend of the radial stress is same with respect to change in the length of the cone.

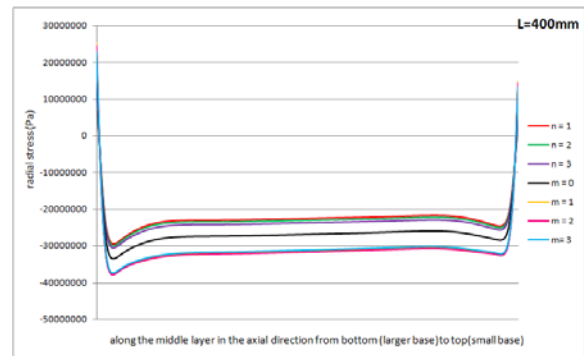


fig.53 distribution of radial stress along the middle layer in the axial direction from bottom(larger base) to top(small base) for L=400mm

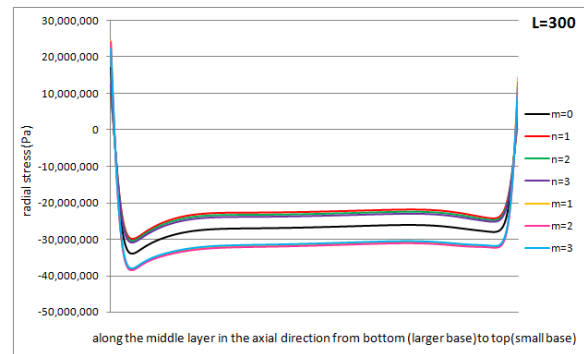


fig.54 distribution of radial stress along the middle layer in the axial direction from bottom(larger base) to top(small base) for L=300mm

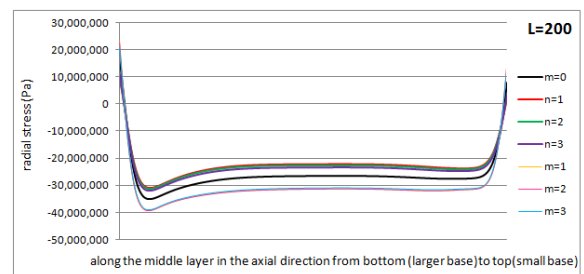


fig.55 distribution of radial stress along the middle layer in the axial direction from bottom(larger base) to top(smaller base) for L=200mm

The set of graphs (fig.56 to fig.58) are the plot between the radial stress and the thickness of the cone along the middle layer in the radial direction from internal to external surface with respect to change in the length of the cone. Radial compressive stress decreases from inner to outer end. Radial stress for m series is greater than that of n series. The stress distribution of the homogeneous material is in between the distribution curves of  $(n, m) > 0$ . As the length of the cone is increased the magnitude of the compressive stress remains unchanged. Variation trend of the radial stress is same with respect to change in the length of the cone.

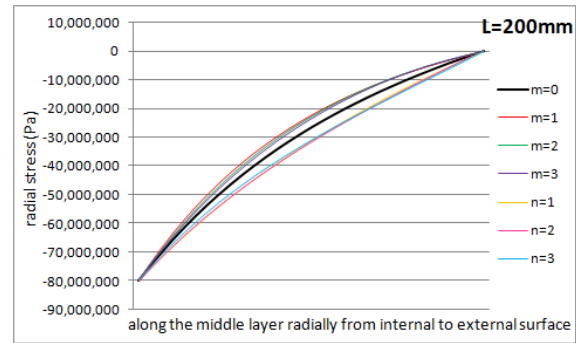


fig.58 distribution of radial stress along the middle layer from internal to the external surface L=200mm

#### 4.2.2.2. Axial stress distribution

The set of graphs (fig.59 to fig. 61) are the plot between the axial stress and the length of the cone along the middle layer in the axial direction (from bottom (larger base) to top (small base)) with respect to change in the length of the cone. Axial stress decreases radially from inner surface to the outer surface with a fluctuation near the bases. Stress for n series is greater than that of m series where as the trend is reversed at the ends (bases). The stress distribution of the homogeneous material is in between the distribution curves of  $(n, m) > 0$ . Intensity of stress decreases with increase in the length of the cone. Variation trend of the axial stress is same with respect to change in the length of the cone.

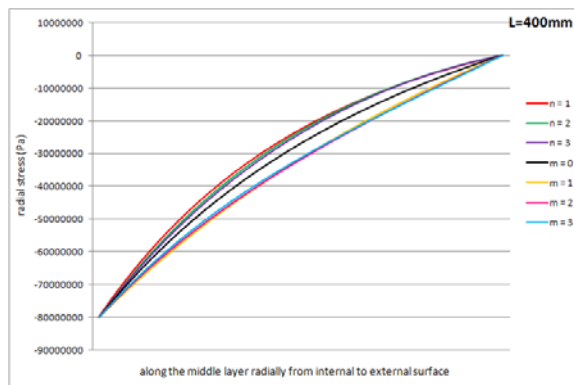


fig.56 distribution of radial stress along the middle layer from internal to the external surface L=400mm

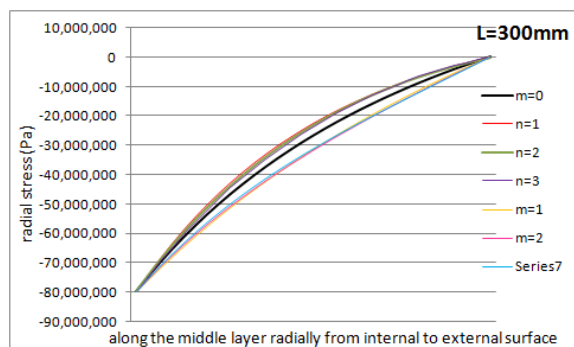


fig.57 distribution of radial stress along the middle layer from internal to the external surface L=300mm

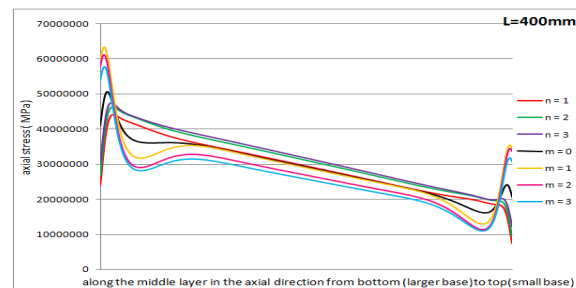


fig.59 distribution of axial stress along the middle layer in the axial direction from bottom(larger base) to top(smaller base) for L=400mm

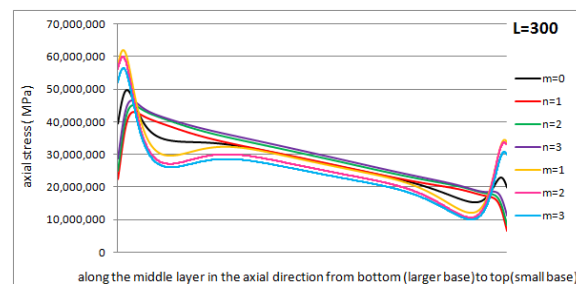


fig.60 distribution of radial stress along the middle layer in the axial direction from bottom(larger base) to top(small base) for L=300mm

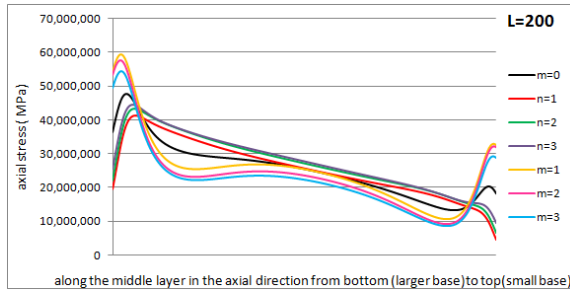


fig.61 distribution of radial stress along the middle layer in the axial direction from bottom(larger base) to top(small base) for L=200mm

The set of graphs (fig.62 to fig.64) are the plot between the axial stress and the thickness of the cone along the middle layer in the radial direction from internal to external surface with respect to change in the length of the cone. Axial stress is more for  $n= 1, 2$  & 3 at the inner half along the thickness (0 to  $h/2$ ) and low for  $m= 1, 2$  & 3. The trend is reverse along outer half along the thickness ( $h/2$  to  $h$ ) i.e. the axial stress is low for  $n= 1, 2$  & 3 and more for  $m= 1, 2$  & 3. The stress distribution of the homogeneous material is almost constant and it is in between the distribution curves of  $(n, m) > 0$ . Intensity of stress decreases with increase in the length of the cone. Variation trend of the axial stress is same with respect to change in the length of the cone.

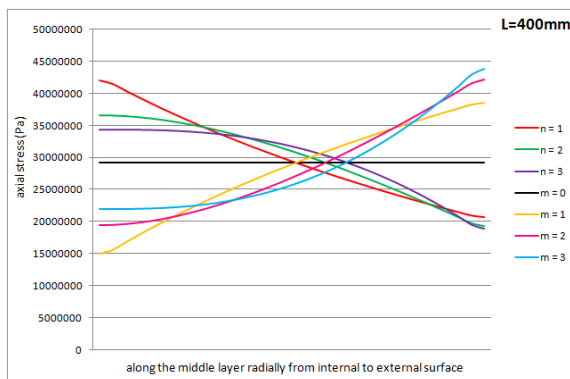


fig.62 distribution of axial stress along the middle layer from internal to the external surface L=400mm

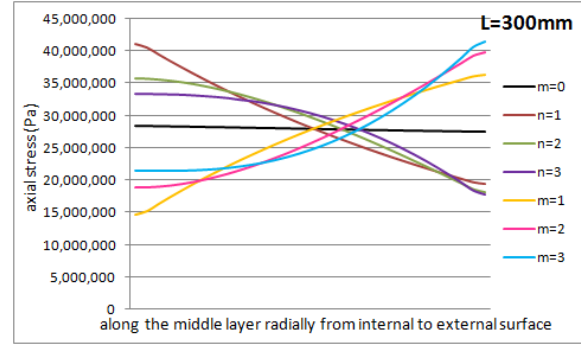


fig.63 distribution of axial stress along the middle layer from internal to the external surface L=300mm

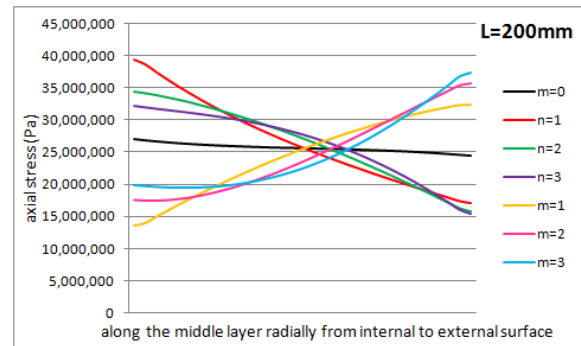


fig.64 distribution of axial stress along the middle layer from internal to the external surface L=200mm

#### 4.2.2.3. Hoop stress

The set of graphs (fig.65 to fig.67) are the plot between the hoop stress and the length of the cone along the middle layer in the axial direction (from bottom (larger base) to top (small base)) with respect to change in the length of the cone. Hoop stress (along the middle layer in axial direction) increases rapidly (from the larger base) attains a maximum value near to the larger base and then slowly reduces (till the near end of the smaller base) and decreases. Stress for  $n$  series is greater than that of  $m$  series. The stress distribution of the homogeneous material is in between the distribution curves of  $(n, m) > 0$ . From the graphs we can infer that, as the length of the cone increases, hoop stress reduces slightly. Change in hoop stress is significant at the bases. Variation trend of the hoop stress is same with respect to change in the length of the cone.

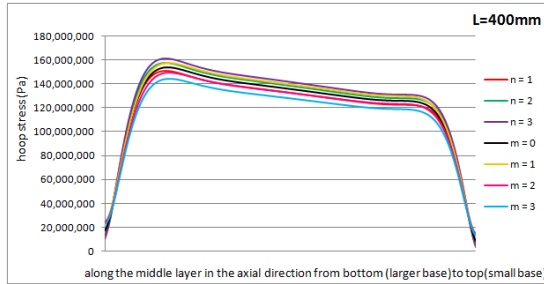


fig.65 distribution of hoop stress along the middle layer in the axial direction from bottom(larger base) to top(small base) for L=400mm

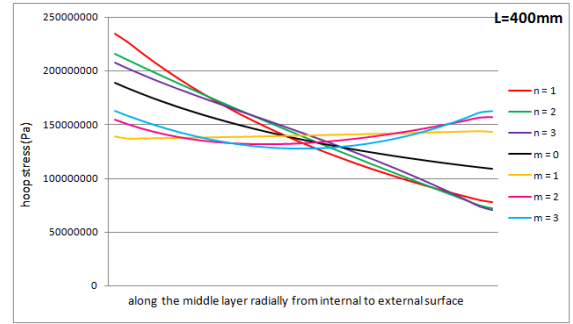


fig.68 distribution of hoop stress along the middle layer from internal to the external surface L=400mm

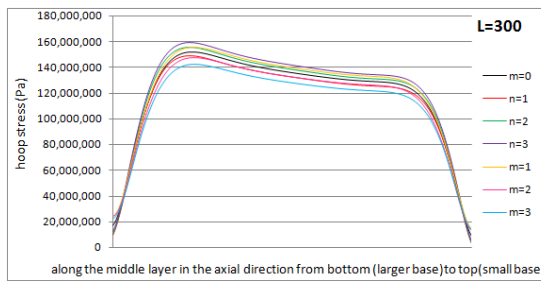


fig.66 distribution of hoop stress along the middle layer in the axial direction from bottom(larger base) to top(small base) for L=300mm

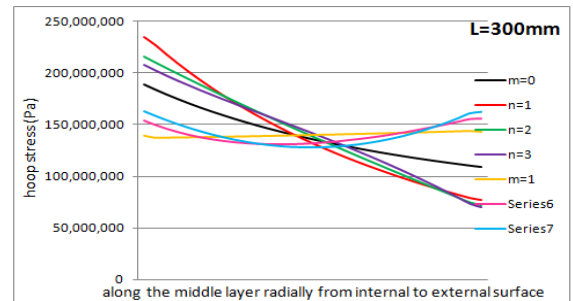


fig.69 distribution of hoop stress along the middle layer from internal to the external surface L=300mm

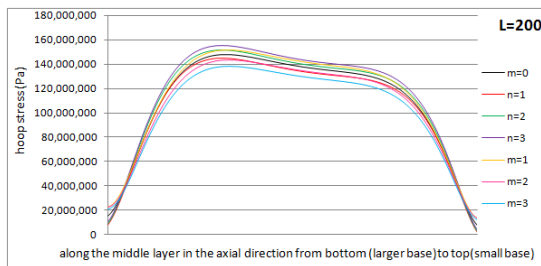


fig.67 distribution of hoop stress along the middle layer in the axial direction from bottom(larger base) to top(small base) for L=200mm

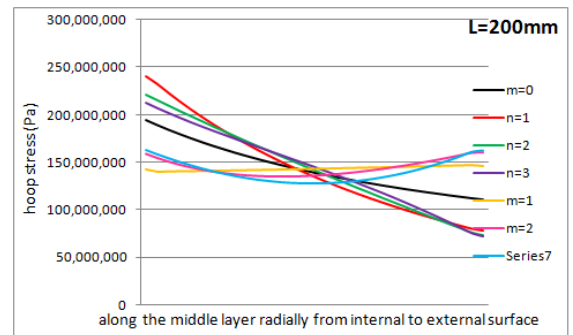


fig.70 distribution of hoop stress along the middle layer from internal to the external surface L=200mm

The set of graphs (fig.68 to fig.70) are the plot between the hoop stress and the thickness of the cone along the middle layer in the radial direction from internal to external surface with respect to change in the length of the cone. Hoop stress is more for  $n = 1, 2$  &  $3$  at the inner half along the thickness ( $0$  to  $h/2$ ) and low for  $m = 1, 2$  &  $3$ . The trend is reverse along outer half along the thickness ( $h/2$  to  $h$ ) i.e. the axial stress is low for  $n = 1, 2$  &  $3$  and more for  $m = 1, 2$  &  $3$ . The stress distribution of the homogeneous material is in between the distribution curves of  $(n, m) > 0$ . Intensity of stress increases in very small amount with increase in the length of the cone. Variation trend of the hoop stress is same with respect to change in the length of the cone.

#### 4.2.2.4. shear stress distribution

The set of graphs (fig.71 to fig.73) are the plot between the shear stress and the length of the cone along the middle layer in the axial direction (from bottom (larger base) to top (small base)) with respect to change in the length of the cone. Maximum stress is induced at the near end of larger base and rapidly reduces to negative shear stress. Then remains almost constant and rapidly decreases to maximum negative stress at the smaller base. Shear stress is same for homogeneous as well as FGM's with  $(n, m) = 1, 2$  &  $3$ . From the graphs we can infer that, as the length of the cone increases, shear stress varies but

the maximum magnitude of the stress is almost same with respect to change in the length of the cone. Variation trend of the shear stress is same with respect to change in the length of the cone.

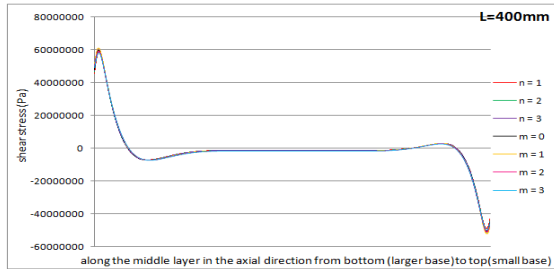


fig.71 distribution of shear stress along the middle layer in the axial direction from bottom(larger base) to top(small base) for L=400mm

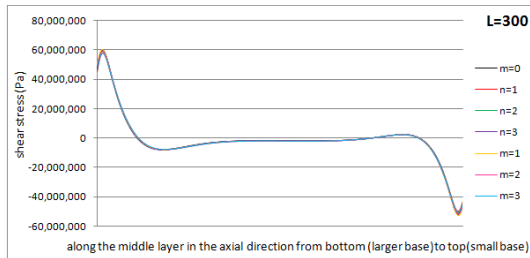


fig.72 distribution of shear stress along the middle layer in the axial direction from bottom(larger base) to top(small base) for L=300mm

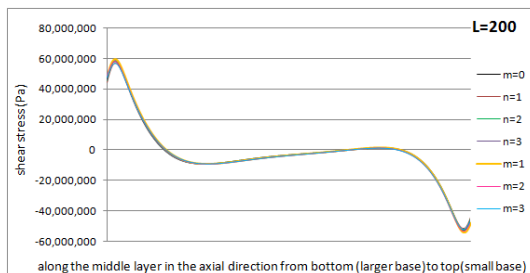


fig.73 distribution of shear stress along the middle layer in the axial direction from bottom(larger base) to top(small base) for L=200mm

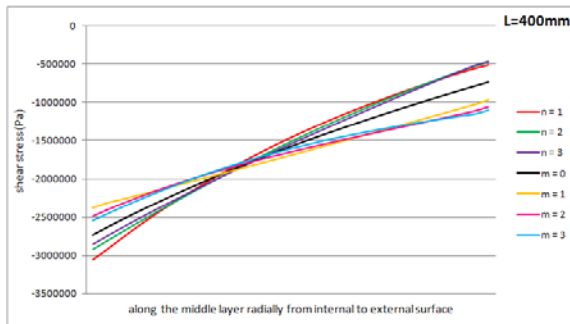


fig.74 distribution of shear stress along the middle layer from internal to the external surface L=400mm

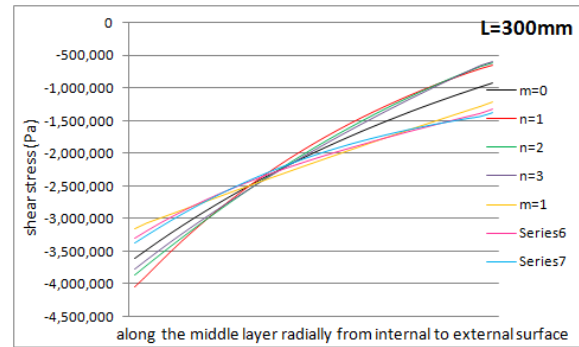


fig.75 distribution of shear stress along the middle layer from internal to the external surface L=300mm

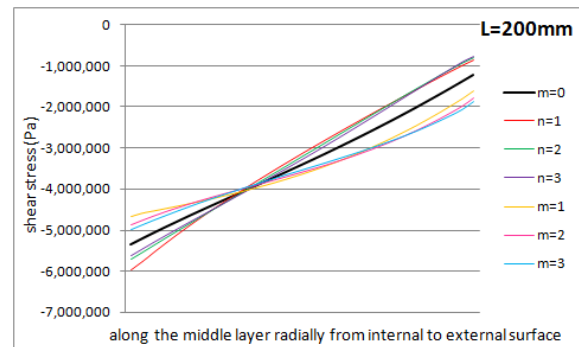


fig.76 distribution of shear stress along the middle layer from internal to the external surface L=200mm

The set of graphs (fig.74 to fig.76) are the plot between the shear stress and the thickness of the cone along the middle layer in the radial direction from internal to external surface with respect to change in the length of the cone. Shear stress is more for  $n = 1, 2 \text{ \& } 3$  at the inner half along the thickness ( $0$  to  $h/2$ ) and low for  $m = 1, 2 \text{ \& } 3$ . The trend is reverse along outer half along the thickness ( $h/2$  to  $h$ ) i.e. the axial stress is low for  $n = 1, 2 \text{ \& } 3$  and more for  $m = 1, 2 \text{ \& } 3$ . The shear stress distribution of the homogeneous material is in between the distribution curves of  $(n, m) > 0$ . Intensity of stress increases with increase in the length of the cone. The increase is significant near the interior surface. Variation trend of the hoop stress is same with respect to change in the length of the cone.

## 5. Conclusion

In this research, the Functionally graded thick hollow truncated cones, have been solved by Finite Element Analysis and compared with homogeneous thick hollow truncated cones. At the boundary areas of the shell with clam-clamp ends the displacement and

stresses are different from the other portion. The conical shells made of positive values of  $n$  have better behavior than the positive values of  $m$ , because of less values of displacements. But we can find some clash among the displacement and stresses values among different values of  $n$  and  $m$ . Analysis has been done by varying the dimensions of the hollow cone. The results obtained for the varied dimensions are then compared. Thus one has to be cautious while selecting the value of  $n$  to attain ergonomics. One can utilize these curves to compare the results obtained from any other numerical or analytical techniques.

## References

- [1]. Yamanouchi, M., Koizumi, M., Hirai, T., Shiota, I.: Proceedings of the First International Symposium on Functionally Graded Materials. Japan (1990)
- [2]. Koizumi, M.: The concept of FGM. Ceram. Trans., Funct. Gradient Mater. **34**, 3–10 (1993)
- [3]. Li, X.F., Peng, X.L.: A pressurized functionally graded hollow cylinder with arbitrarily varying material properties. J. Elast. **96**, 81–95 (2009)
- [4]. Chen, Y.Z., Lin, X.Y.: Elastic analysis for thick cylinders and spherical pressure vessels made of functionally graded materials. Comput. Mater. Sci. **44**, 581–587 (2008)
- [5]. Hongjun, X., Zhifei, S., Taotao, Z.: Elastic analyses of heterogeneous hollow cylinders. Mech. Res. Commun. **33**, 681–691 (2006)
- [6]. Fukui, Y., Yamanaka, N.: Elastic analysis for thick-walled tubes of functionally graded material subjected to internal pressure. JSME Int. J. Ser. I **35**(4), 379–385 (1992)
- [7]. Tutuncu, N., Ozturk, M.: Exact solutions for stresses in functionally graded pressure vessels. Compos. Part B Eng. **32**(8), 683–686 (2001)
- [8]. Tutuncu, N.: Stresses in thick-walled FGM cylinders with exponentially-varying properties. Eng. Struct. **29**, 2032–2035 (2007)
- [9]. Zamani Nejad, M., Rahimi, G.H.: Elastic analysis of FGM rotating cylindrical pressure vessels. J. Chinese Institute of Engineers. **33**(4), (2010, in press)
- [10]. Ghannad, M., Zamani Nejad, M., Rahimi, G.H.: Elastic solution of axisymmetric thick truncated conical shells based on first-order shear deformation theory. MECHANIKA. **79**(5), ISSN 1392-1207 (2009)
- [11]. Horgan, C.O.: The pressurized hollow cylinder or disk problem for functionally graded isotropic linearly elastic materials. J. Elast. **55**, 43–59 (1999)
- [12]. Nie, G.J., Batra, R.C.: Exact solutions and material tailoring for functionally graded hollow circular cylinders. J. Elast. **99**, 179–201 (2010)
- [13]. Jabbari, M., Sohrabpour, S., Eslami, M.R.: Mechanical and thermal stresses in functionally graded hollow cylinder due to radially symmetric loads. Int. J. Press. Vessels Piping **79**, 493–497 (2002)
- [14]. Jabbari, M., Bahtui, A., Eslami, M.R.: Axisymmetric mechanical and thermal stresses in thick short length FGM cylinders. Int. J. Press. Vessels Piping **86**, 296–306 (2009)
- [15]. M. Ghannad, H. Gharooni Displacements and Stresses in Pressurized Thick FGM Cylinders with Varying Properties of Power Function Based on HSDT *Journal of Solid Mechanics Vol. 4, No. 3 (2012) pp. 237-251 (2012)*
- [16]. G. F. Hausenbauer and G. C. Lee, “Stresses in thick-walled conical shells,” Nuclear Engineering and Design, vol. 3, no. 3, pp. 394–401, 1966.
- [17]. I. S. Raju, G.V.Rao, B. P.Rao, and J. Venkataramana, “A conical shell finite element,” *Computers and Structures*, vol. 4, no. 4, pp. 901–915, 1974
- [18]. S. Takahashi, K. Suzuki, and T. Kosawada, “Vibrations of conical shells with variable thickness,” Bulletin of the JSME Japan Society of Mechanical Engineers, vol. 29, no. 258, pp. 4306–4311, 1986.
- [19]. B. S. K. Sundarasivarao and N. Ganesan, “Deformation of varying thickness of conical shells subjected to axisymmetric loading with various end conditions,” *Engineering Fracture Mechanics*, vol. 39, no. 6, pp. 1003–1010, 1991.
- [20]. S. A. Tavares, “Thin conical shells with constant thickness and under axisymmetric load,” *Computers and Structures*, vol. 60, no. 6, pp. 895–921, 1996.
- [21]. W. Cui, J. Pei, and W. Zhang, “Simple and accurate solution for calculating stresses in conical shells,” *Computers and Structures*, vol. 79, no. 3, pp. 265–279, 2001.
- [22]. C.-P. Wu and S.-J. Chiu, “Thermally induced dynamic instability of laminated composite conical shells,” *International Journal of Solids and Structures*, vol. 39, no. 11, pp. 3001–3021, 2002.
- [23]. I. F. Pinto Correia, C. M. Mota Soares, C. A. Mota Soares, and J. Herskovits, “Analysis of laminated conical shell structures using higher order models,” *Composite Structures*, vol. 62, no. 3-4, pp. 383–390, 2003.
- [24]. C.-P. Wu, Y.-F. Pu, and Y.-H. Tsai, “Asymptotic solutions of axisymmetric laminated conical shells,” *Thin-Walled Structures*, vol. 43, no. 10, pp. 1589–1614, 2005.
- [25]. H. R. S. Eipakchi, E. Khadem, and G.H. S. Rahimi, “Axisymmetric stress analysis of a thick conical shell with

varying thickness under nonuniform internal pressure,” *Journal of Engineering Mechanics*, vol. 134, no. 8, pp. 601–610, 2008.

[26]. M. Ghannad, M. Z. Nejad, and G. H. Rahimi, “Elastic solution of axisymmetric thick truncated conical shells based on firstorder shear deformation theory,” *Mechanika*, vol. 79, no. 5, pp. 13–20, 2009.

[27]. H. R. Eipakchi, “Third-order shear deformation theory for stress analysis of a thick conical shell under pressure,” *Journal of Mechanics of Materials and Structures*, vol. 5, no. 1, pp. 1–17, 2010.

[28]. K. Asemi, M. Akhlaghi, M. Salehi, and S. K. Hosseini Zad, “Analysis of functionally graded thick truncated cone with finite length under hydrostatic internal pressure,,” vol. 81, no. 8, pp. 1063–1074, 2011.

[29]. M. Ghannad and M. Zamani Nejad, “Elastic analysis of pressurizedthick hollow cylindrical shells with clamped-clampedends,” *Mechanika*, vol. 85, no. 5, pp. 11–18, 2010.

[30]. M. Z. Nejad, M. Jabbari, and M. Ghannad, “A semi-analytical solution for elastic analysis of rotating thick cylindrical shells with variable thickness using disk form multilayers,” *The ScientificWorld Journal*, vol. 2014, Article ID 932743, 10 pages, 2014.

[31]. Shakeri, M., Akhlaghi, M., Hoseini, S.M.: Vibration and radial wave propagation velocity in fuctionally graded thick hollow cylinder. *Structures* **76**, 174–181 (2006)

[32]. "Stress Analysis of Pressurized Thick Truncated Conical Shells with varying Modulus of Elasticity as Power Function", *Trends in Mechanical Engineering & Technology* ISSN: 22311793 (online), ISSN: 23479965 (print) Volume 4, Issue 3 [www.stmjournals.com](http://www.stmjournals.com). P. Aravinda Sai Murthy, N. D. Mittal Department of Mechanical Engineering, Maulana Azad National Institute of Technology, Bhopal (M.P.), India.

**First author:** P Aravinda sai murthy, pursuing M. Tech in MANIT under the department of Mechanical Engineering in the specialization 'Engineering Materials'.

**Second author:** Dr. N.D. Mittal, Professor in the Department of Mechanical Engineering, MANIT. Visited to University of Huddersfield (U.K.) for training in Educational Technology, 1996. Acted as Honorary Secretary, Institution of Engineers (India) MP state center for 2002 - 2003. Executive Member National Committee of ISTAM 1995 – 1997.